Saudi Journal of Biological Sciences 29 (2022) 3456–3465

Contents lists available at ScienceDirect

Saudi Journal of Biological Sciences

journal homepage: www.sciencedirect.com

Original article

Phytocompounds as potential inhibitors of SARS-CoV-2 Mpro and PLpro through computational studies

Mithun Rudrapal [a,*], Ismail Celik [b], Sampath Chinnam [c], Mohammad Azam Ansari [d], Johra Khan [e,f], Saad Alghamdi [g], Mazen Almehmadi [h], James H. Zothantluanga [i], Shubham J. Khairnar [j]

[a] Department of Pharmaceutical Chemistry, Rasiklal M. Dhariwal Institute of Pharmaceutical Education & Research, Pune 411019, Maharashtra, India
[b] Department of Pharmaceutical Chemistry, Faculty of Pharmacy, Erciyes University, Kayseri 38280, Turkey
[c] Department of Chemistry, M. S. Ramaiah Institute of Technology (Affiliated to Visvesvaraya Technological University, Belgaum), Bengaluru 560054, Karnataka, India
[d] Department of Epidemic Disease Research, Institute for Research and Medical Consultations (IRMC), Imam Abdulrahman Bin Faisal University, Dammam 31441, Saudi Arabia
[e] Department of Medical Laboratory Sciences, College of Applied Medical Sciences, Majmaah University, Al Majmaah 11952, Saudi Arabia
[f] Health and Basic Sciences Research Center, Majmaah University, Al Majmaah 11952, Saudi Arabia
[g] Laboratory Medicine Department, Faculty of Applied Medical Sciences, Um Al-Qura University, Makkah 24382, Saudi Arabia
[h] Department of Clinical Laboratory Sciences, College of Applied Medical Sciences, Taif University, Taif 21944, Saudi Arabia
[i] Department of Pharmaceutical Sciences, Faculty of Science and Engineering, Dibrugarh University, Dibrugarh 786004, Assam, India
[j] MET Institute of Pharmacy, Bhujbal Knowledge City, Nasik 422003, Maharashtra, India

ARTICLE INFO

Article history:
Received 5 January 2022
Revised 4 February 2022
Accepted 20 February 2022
Available online 25 February 2022

Keywords:
SARS-CoV-2
Mpro
PLpro
Spice phytochemicals
Molecular docking
Molecular dynamics

ABSTRACT

The inhibition of severe acute respiratory syndrome coronavirus 2 (SARS-CoV-2) main protease (Mpro) and papain-like protease (PLpro) prevents viral multiplications; these viral enzymes have been recognized as one of the most favorable targets for drug discovery against SARS-CoV-2. In the present study, we screened 225 phytocompounds present in 28 different Indian spices to identify compounds as potential inhibitors of SARS-CoV-2 Mpro and PLpro. Molecular docking, molecular dynamics simulation, molecular mechanics Poisson–Boltzmann surface area (MM-PBSA) binding free energy calculations, and absorption, distribution, metabolism, excretion and toxicity (ADMET) studies were done. Based on binding affinity, dynamics behavior, and binding free energies, the present study identifies pentaoxahexacyclo-dotriacontanonaen-trihydroxybenzoate derivative (PDT), rutin, and dihyroxy-oxanphenyl-chromen-4-one derivative (DOC), luteolin-7-glucoside-4′-neohesperidoside as promising inhibitors of SARS-CoV-2 Mpro and PLpro, respectively.

1. Introduction

Among many disease outbreaks caused by RNA viruses, coronavirus disease 2019 (COVID-19) caused by severe acute respiratory syndrome coronavirus 2 (SARS-CoV-2) is by far, the deadliest of all (Rudrapal et al., 2021a; Mohamadian et al., 2021; Khan et al., 2021). Since its initial in December 2019, COVID-19 has afflicted human lives worldwide (Liu et al., 2020; Dong et al., 2020; Rudrapal et al., 2020). Current pharmacotherapies available for COVID-19 have their share of controversy with some studies reporting their effectiveness while others are reporting the opposite. The emergence of different new variants, different reports on vaccine side effects, and the global issue of vaccine hesitancy are some other serious issues that have put the world in a state of dilemma as they had crippled our fight against COVID-19 to a certain degree (Lucia et al., 2021; Riad, 2021). These problems mandate the urgent need to find an alternative treatment strategy that will supplement the current treatment regimens of COVID-19.

Viral enzymes such as the main protease (Mpro) and papain-like protease (PLpro) are significantly responsible for the replication of SARS-CoV-2 (Rudrapal et al., 2022). As inhibition of Mpro and PLpro prevents viral multiplication, they have been recognized as the most favorable targets for anti-SARS-CoV-2 drugs (Dror et al., 2020; Bhat et al., 2020; Kumar et al., 2021a). Medicinal plants and their phytoconstituents have been proposed as potential phytotherapy for COVID-19 (Prajapati et al., 2021). The polyphenolic-

* Corresponding author.
E-mail address: rsmrpal@gmail.com (M. Rudrapal).
Peer review under responsibility of King Saud University.

Production and hosting by Elsevier

https://doi.org/10.1016/j.sjbs.2022.02.028
1319-562X/

rich extract of *Vitis vinifera* (grapevine) has been reported to act (*in vitro*) against SARS-CoV-2 (Zannella et al., 2021). It is safe to state that medicinal plants hold tremendous potential to be developed as alternative phytotherapy for COVID-19. Nowadays, computational techniques are being extensively used to investigate the inhibitory potential of phytocompounds against SARS-CoV-2 (Sachdeva et al., 2020; Shah et al., 2020). Several studies conclude that phytocompounds can potentially inhibit the Mpro and PLpro of SARS-CoV-2 (Gowrishankar et al., 2021; Kumar et al., 2020). In the drug discovery process, computational techniques including docking and molecular dynamics (MD) simulation offer several advantages owing to their efficiency, accuracy, robustness, and eco-friendly approach (Hassan Baig et al., 2016).

Spices are used to enrich the flavor and aroma of our daily diet. Ginger, rosemary, onion, turmeric, cloves, fennelflower, black pepper, garlic, clove, cinnamon, coriander, and basil are a few examples among many other consumed spices in India. Spices contain several bioactive compounds that are used for the management of inflammatory diseases, cardiovascular diseases, cancer, metabolic diseases and viral infections (Srinivasan, 2005; Embuscado, 2019; Opara and Chohan, 2014; Yashin et al., 2017). In the study, a total of 225 phytocompounds present in 28 Indian spices were computationally investigated for their inhibitory action against SARS-CoV-2 by carrying out molecular docking, MD simulation, and binding free energy calculations against Mpro and PLpro.

2. Materials and methods

2.1. Retrieval of target proteins

The proteins structures of SARS-CoV-2 were retrieved from the RCSB-PDB website. The Mpro (PDB id: 6 W63, 2.1 Å) and PLpro (PDB id: 7JIW, 2.3 Å) bear the co-crystal inhibitors of X77 and VBY, respectively.

2.2. Preparation of proteins

The preparation of proteins was initiated with the removal of water molecules using the Schrodinger suite Maestro (version 2021–2). The residues involving side chain amino acids were filled, the missing hydrogen atoms were added, and the H-bonds were optimized. The OPLS4 force field was applied for minimization of energy until the root-mean-square deviation (RMSD) value averages at 0.30 Å (Roos et al., 2019; Kumar et al., 2021b).

2.3. Preparation of ligands

The chemical structures of phytocompounds present in Indian spices were obtained from an online database, COCONUT (https://coconut.naturalproducts.net/). The LipPrep module of Schrodinger was used to prepare the 3-dimensional (3D) coordinates of all the phytocompounds (Chen and Foloppe, 2010). The Epik module of Schrodinger suite version 2021–2 was used to achieve an ionization state of pH 7.4, and the tautomer and chirality were also predicted. Energy minimization was carried out with OPLS4 force field and the process was allowed to proceed until the conformation obtained was energetically stable (Roos et al., 2019).

2.4. Molecular docking

A compound library of 225 phytocompounds found to be present in Indian spices was studied for their binding affinity towards Mpro and PLpro by molecular docking study (MDS). The glide docking module of Schrodinger Maestro which uses the extra precision (XP) protocol was used for MDS (Friesner et al., 2006; Chen and Foloppe, 2010). Considering the position of the co-crystallized ligand (Kalita et al. 2020), the binding site in the protein was identified with the application of default settings to the glide-receptor grid generation module (Halgren et al., 2004).

Following the same protocol as described above, the native ligands were re-docked into the same binding pocket where they were originally present. This was done to validate the docking protocol to examine if the specified methods used in the present MDS will be able to dock the test compounds into the same binding pocket where the native ligand was initially present. The RMSD value between the original docked ligand and the re-docked ligand was calculated (Hevener et al., 2009).

2.5. Molecular dynamics simulation

Molecular dynamics (MD) simulation was carried out with GROMACS 2019.2 software (Abraham et al., 2015; Rath et al., 2021; Ghosh et al., 2021; Pasala et al., 2022). The GROMOS96 54a7 force field was then applied for energy minimization. The SCP water model was used for salvation of protein–ligand complexes. The 'gmxgenion' script was used to electrically neutralize the solvated model by adding chloride ions and sodium ions. Following this, it was equilibrated with 0.3 ns isothermal-isobaric (NPT) and 0.3 ns isothermal-isochoric (NVT) ensembles. The simulation period was for 100 ns. The motion equation was integrated into triplicates with the leapfrog algorithm at 2 fs time step. GROMACS scripts were used to generate the trajectories such as RMSD, RMSF, and radius of gyration (Rg) (Swargiary et al., 2020; Junejo et al., 2021). Visual molecular dynamics 1.9.3 was used for visualization and analysis of trajectories (Humphrey et al., 1996).

2.6. Molecular mechanics Poisson–Boltzmann surface area (MM-PBSA) binding free energy calculations

The MM-PBSA was used to quantify the binding (free) energies of complexes using the g_mmpbsa script (Kumari et al., 2014; James et al., 2022). Energies of Van der Waals, polar solvation, electrostatic, and non-polar energy i.e., solvent-accessible surface area (SASA) were calculated.

2.7. Absorption, distribution, metabolism, excretion and toxicity (ADMET) prediction studies

Lipinski's rule of 5, bioavailability score, and synthetic accessibility score were studied with the SwissADME web tool (Daina et al., 2017). The median lethal dose (LD_{50}) and toxicity class of the phytocompounds were computed with ProTox-II web tool (Banerjee et al., 2018). The drug score was obtained using DataWarrior v.5.2.1 software.

3. Results

3.1. Molecular docking

MDS revealed the binding affinity of the studied phytocompounds for the active sites of the target enzymes. A high binding affinity indicated by low binding energy involvement is considered as an important factor for selecting compounds to be further studied. The XP glide score of 10 phytocompounds that showed the best binding affinity towards the Mpro and PLpro is given in Table 1. The glide score of the native ligands originally bound to the target protein is also given in Table 1. PDT (COCONUT ID: CNP0412082), and rutin (COCONUT ID: CNP0268715) have the best docking score for Mpro. The glide score of PDT and rutin are −15.367 and −12.360, respectively, while that of the native ligand

Table 1
Glide XP docking results against Mpro and PLpro of SARS-CoV-2 Mpro: main protease; PLpro: papain-like protease.

Target protein	COCONUT ID	Glide model (kcal/mol)	XP glide score (kcal/mol)
Mpro	CNP0412082	−133.394	−15.367
	CNP0268715	−88.446	−12.360
	CNP0301186	−93.129	−12.218
	CNP0218615	−94.339	−11.566
	CNP0152789	−85.227	−10.810
	CNP0239834	−119.231	−10.676
	CNP0222584	−78.242	−10.162
	CNP0008956	−75.654	−9.328
	CNP0330206	−53.498	−8.825
	CNP0144084	−81.929	−7.972
	X77	−85.045	−5.966
PLpro	CNP0301186	−81.550	−12.801
	CNP0359835	−85.978	−9.226
	CNP0152789	−74.222	−9.148
	CNP0289609	−49.572	−7.471
	CNP0289609	−49.572	−7.471
	CNP0245197	−57.849	−7.100
	CNP0120486	−64.110	−7.094
	CNP0195904	−45.290	−7.081
	CNP0239834	−90.872	−6.390
	CNP0115940	−56.870	−6.315
	VYB	−86.452	−6.538

(X77) is −5.966. DOC (COCONUT ID: CNP0301186), and luteolin-7-glucoside-4′-neohesperidoside (COCONUT ID: CNP0359835) have the best docking score for PLpro. The glide score of DOC and luteolin-7-glucoside-4′-neohesperidoside are −12.801 and −9.226, respectively, while that of the native ligand (VYB) is −6.538.

The re-docking method used for the validation of docking study was successful. This process was carried out to see the accuracy and efficiency of the docking method adopted for the study. For Mpro and PLpro, the computed RMSD values between the original inhibitor and the re-docked inhibitor were 2.498 Å and 0.385 Å, respectively.

3.2. Analyses of protein–ligand interactions

3.2.1. SARS-CoV-2 Mpro

The 2D and 3D ligand interactions of X77, PDT, and rutin against Mpro are given in Fig. 1. The co-crystal inhibitor X77 formed conventional H-bonds with ASN142, GLY143, HIS163, and GLU166; hydrophobic attractions with HIS41 and LEU27; electrostatic interactions with MET49 and CYS145; and Van der Waals interactions were shown by different amino acid residues (Fig. 1a, b). PDT formed conventional H-bonds with THR24, CYS44, GLY143, CYS145, GLU166, ARG188, and GLN189; hydrophobic attractions with HIS41, MET49, and MET165; and van der Waals interactions were shown by different amino acid residues (Fig. 1c, d). Rutin formed H-bonds with THR26, GLY143, CYS145, GLU166, and ARG188; hydrophobic interaction with MET165; electrostatic interaction with MET49; and Van der Waals interactions were shown by HIS41 along with different amino acid residues (Fig. 1e, f).

3.2.2. SARS-CoV-2 PLpro

The 2D and 3D ligand interactions of VYB, DOC, and luteolin-7-Glucoside-4′-Neohesperidoside against PLpro are given in Fig. 2. The co-crystal inhibitor VYB formed conventional H-bonds with ASP164, GLU167, and GLN269; hydrophobic attractions with PRO247, PRO248, TYR264, and TYR273; and Van der Waals interactions were shown by different amino acid residues (Fig. 2a, b). DOC formed conventional H-bonds with ASP164, GLU167, PRO248, GLY266, and ASN267; hydrophobic attractions with PRO247; and van der Waals interactions were shown by different amino acid residues (Fig. 2c, d). Luteolin-7-Glucoside-4′-Neohesperidoside formed conventional H-bonds with LYS157, GLU161, ASP164, ARG166, GLU167, and THR301; hydrophobic attractions with TYR171 and TYR268; and van der Waals interactions were shown by different amino acid residues (Fig. 2e, f).

3.3. MD simulation

From results of simulation studies, the conformational stability as well as dynamics complex formation was obtained for 100 ns period.

3.3.1. SARS-CoV-2 Mpro

The RMSD, RMSF, and Rg of the co-crystal inhibitor (X77), and the two ligand (PDT and rutin) complexes were plotted as graphs in Fig. 3. The RMSD trajectory of the Mpro-X77 complex showed signs of stability as it fluctuates between 0.1 nm and ∼ 0.3 nm, and the majority of the fluctuations occurred at ∼ 0.2 nm (Fig. 3a). The majority of the RMSD trajectory of the Mpro-rutin complex seemed to fluctuate between 0.2 nm and 0.3 nm and the observed data was indicative of a stable protein–ligand complex (Fig. 3a). After 20 ns, the RMSD trajectory of the Mpro-PDT complex fluctuates around 0.3 nm and ends at 0.4 nm which was suggestive of a stable conformation for the ligand on the binding site of Mpro (Fig. 3a).

The RMSF data of each amino acid residue of SARS-CoV-2 Mpro is plotted in Fig. 3b. During the 100 ns MD simulation, the fluctuation of each amino acid of Mpro-rutin and Mpro-PDT were similar to Mpro-X77. As homogeneity of RMSF was maintained in all complexes, the results obtained from this parameter support and correlate with the RMSD trajectory of the complexes.

The compactness of protein molecule during the simulation period was determined by the Rg. The observed Rg data is given in Fig. 3c. The Rg trajectory of Mpro-X77 fluctuates between 2.15 and 2.25 nm. The Mpro-rutin Rg trajectory fluctuated between 2.20 nm and 2.30 nm for about 50 ns and then stabilized at around 2.25 nm for the rest of the simulation. The majority of the Rg trajectory of Mpro-PDT fluctuated between 2.20 nm and 2.25 nm. The Rg trajectory of rutin and PDT fluctuated within a small unit similar to X77.

3.3.2. SARS-CoV-2 PLpro

The RMSD, RMSF, and Rg of the co-crystal inhibitor (VBY) and the two (luteolin-7-glucoside-4′-neohesperidoside and DOC) complexes were plotted as graphs in Fig. 4. The PLpro-VBY complex RMSD trajectory showed fluctuation between the range of 0.2 nm and 0.4 nm; while the majority of the fluctuations occurred at ∼ 0. 3 nm (Fig. 4a). The RMSD trajectory of the PLpro-luteolin-7-glucoside-4′-neohesperidoside complex fluctuates from 0.2 nm up to 0.4 nm for 20 ns and then stabilized between 0.3 nm and 0.4 nm for the rest of the period (Fig. 4a). After 20 ns, the majority of the RMSD fluctuations of the PLpro-DOC complex occurred between 0.2 5 nm and 0.35 nm, which suggested optimal stability conformation of the ligand while complex formation with PLpro (Fig. 4a).

The RMSF data of PLpro are plotted in Fig. 4b. During the simulation, the fluctuation of each amino acid of PLpro-luteolin-7-glucoside-4′-neohesperidoside and PLpro-DOC were similar to PLpro-VBY. As the homogeneity of RMSF was maintained in all studied complexes, the findings of the RMSF supports and correlate with the RMSD trajectory of all the complexes (Khan et al., 2021).

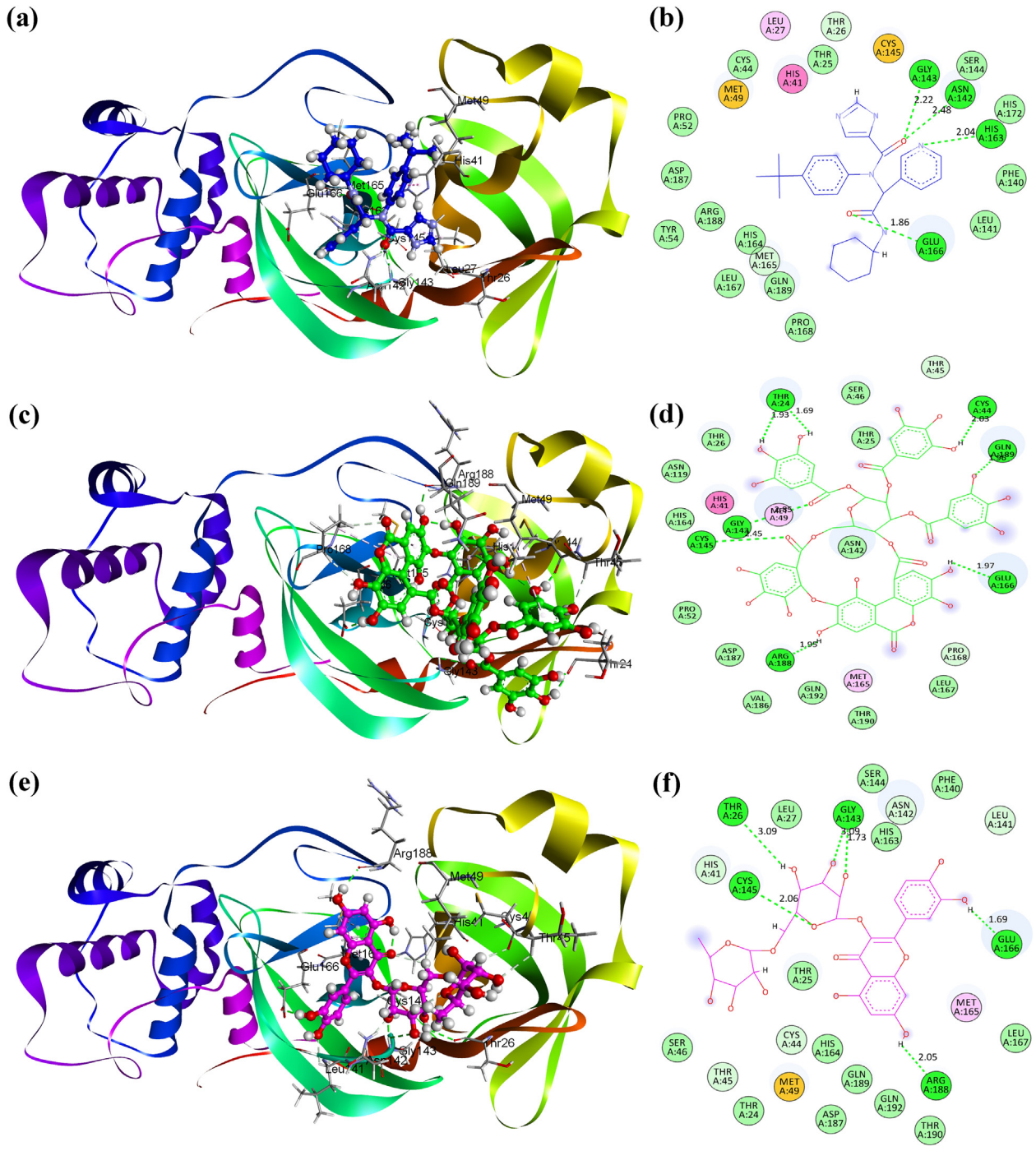

Fig. 1. 2D and 3D ligand interactions of X77, PDT, and rutin against SARS-COV-2 Mpro.

The observed Rg data for PLpro and its ligand complexes is given in Fig. 4c. The Mpro-VBY Rg trajectory fluctuates between 2.20 nm and 2.30 nm for up to 95 ns of MD simulation and fluctuates between 2.15 nm and 2.25 for the last 5 ns. The Rg trajectory of Mpro-luteolin-7-glucoside-4′-neohesperidoside fluctuated between 2.15 nm and 2.30 nm for up to 60 ns and stabilized at around 2.25 nm till end of simulation. A majority of the Rg trajectory of Mpro-DOC fluctuated between 2.20 nm and 2.30 nm for up to 40 ns, stabilized between 2.20 nm and 2.25 nm for up to 95 ns, then ends between 2.25 nm and 2.35 for the last 5 ns. The Rg trajectory of luteolin-7-glucoside-4′-neohesperidoside and DOC fluctuated within a limited unit like VBY.

3.4. MM-PBSA binding free energies

The binding free energy represents the amount of energy generated as a result of protein–ligand interaction (Othman et al., 2021). A more negative binding free energy suggests more effective protein–ligand binding.

3.4.1. SARS-CoV-2 Mpro

The binding energies of complexes with Mpro are given in Table 2. Among the selected complexes, Mpro-PDT (-280.170 ± 18.945 kJ/mol) showed more negative binding energy followed by Mpro-X77 (-160.625 ± 15.840 kJ/mol), and Mpro-rutin complex

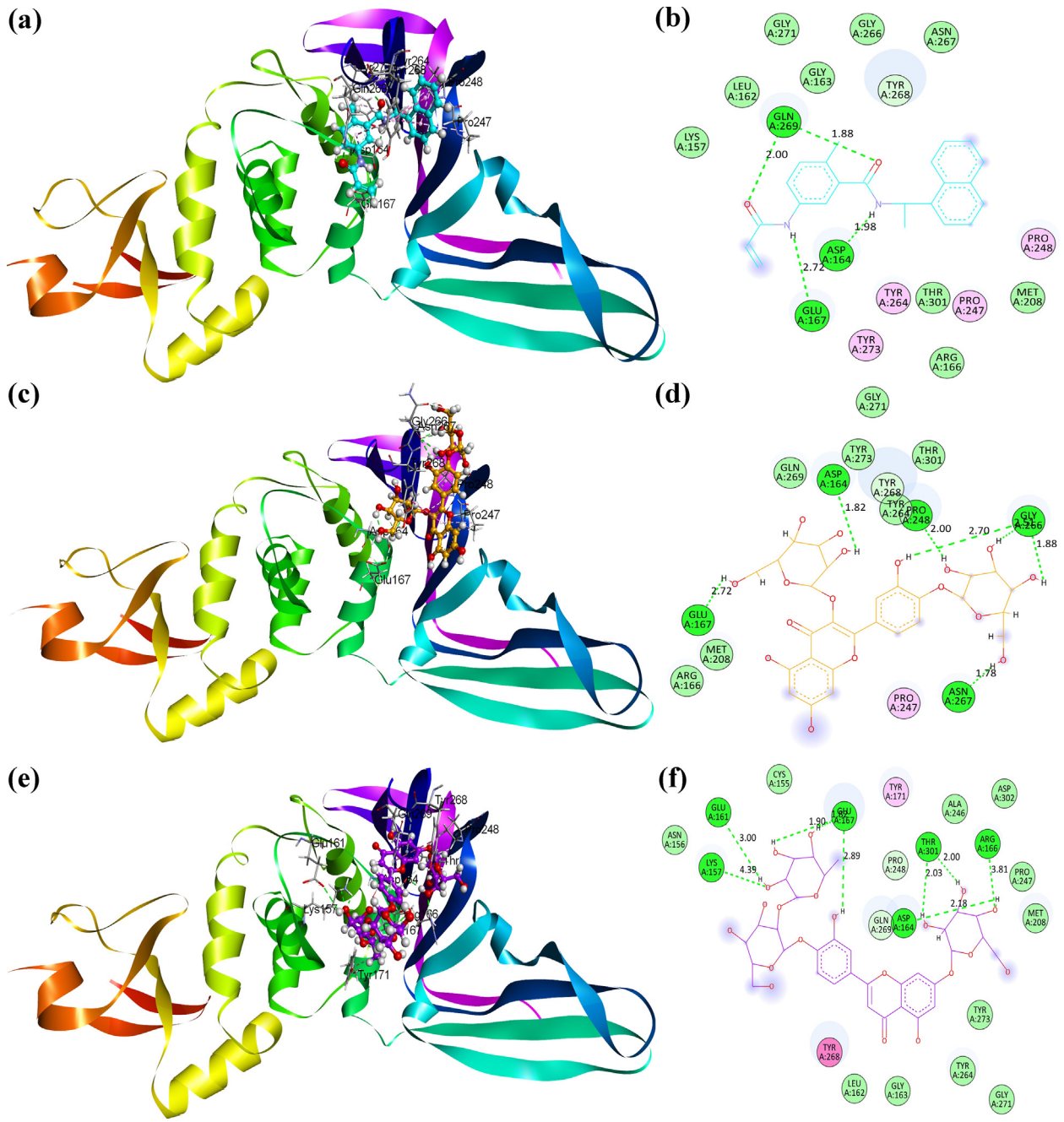

Fig. 2. 2D and 3D ligand interactions of VYB, DOC, and luteolin-7-Glucoside-4′-Neohesperidoside against SARS-CoV-2 PLpro.

(-146.820 ± 15.448 kJ/mol). In terms of binding free energy, PDT outperforms X77, while rutin failed to outperform X77.

3.4.2. SARS-CoV-2 PLpro

The binding free energies of complexes with PLpro are given in Table 3. The binding energy of PLpro-DOC (-148.323 ± 15.338 kJ/mol) is more negative followed by PLpro-luteolin-7-glucoside-4′-neohesperidoside (-142.425 ± 22.452 kJ/mol), and PLpro-VBY (-141.573 ± 13.971 kJ/mol). Both DOC and luteolin-7-glucoside-4′-neohesperidoside outperform the native ligand of the protein.

3.5. ADMET properties

The ADMET parameters of the studied compounds are given in Table 4. All of the selected compounds violated 3 rules of Lipinski's rule of 5 (molecular weight > 500, hydrogen acceptor > 10, hydrogen donor > 5), and each has a bioavailability score of 0.17. A low synthetic accessibility score means the compound will be easy to synthesize. Rutin (6.52) has the lowest synthetic accessibility score followed by DOC (6.54), luteolin-7-glucoside-4′-neohesperidoside (7.48), and PDT (8.43). The LD_{50} of PDT was 2250 mg/kg body weight and 5000 mg/kg was the LD_{50} for rutin, DOC, and luteolin-7-glucoside-4′-neohesperidoside. All compounds belonged to toxicity class 5 that suggests their safety for oral consumption. Rutin (0.546604) has the highest drug score followed by PDT (0.2016708), DOC (0.1766791), and luteolin-7-glucoside-4′-neohesperidoside (0.1573803).

4. Discussion

In an attempt to find out molecules that could control the multiplication of SARS-CoV-2, several computational studies have been

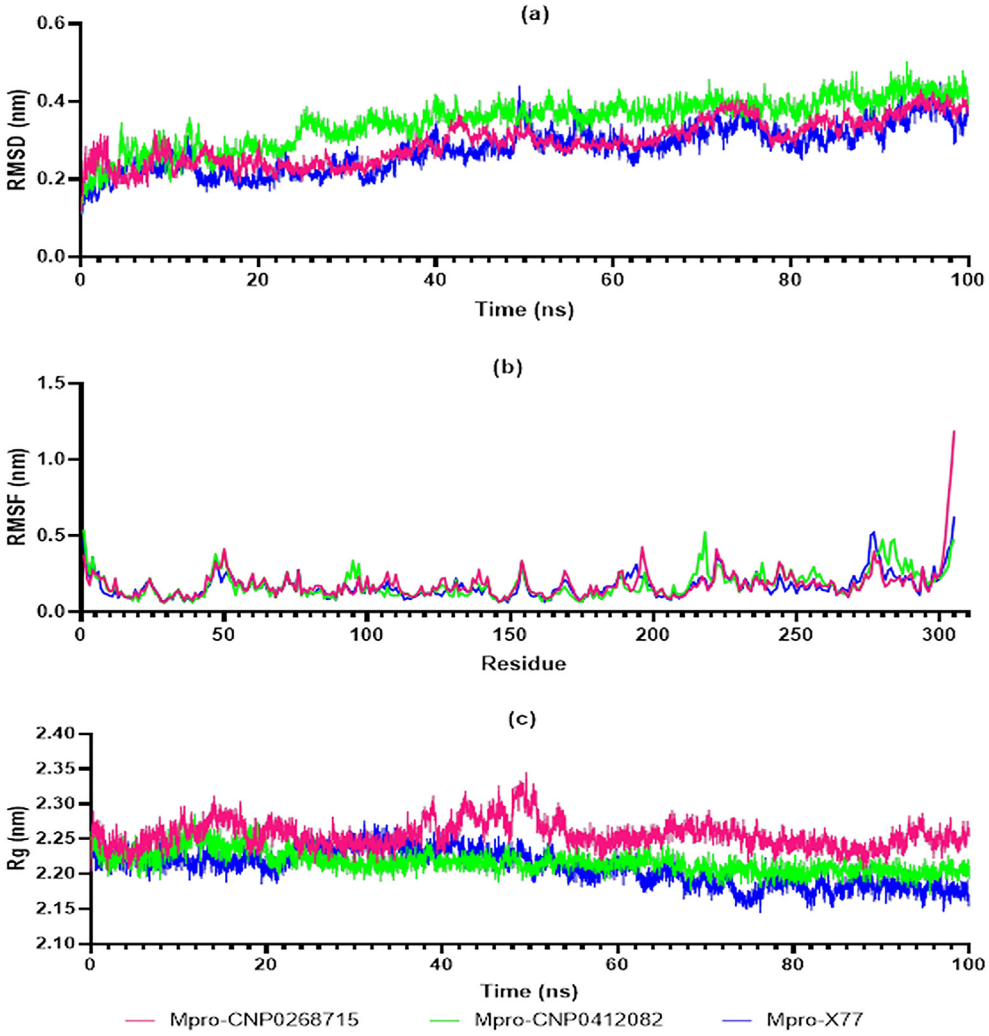

Fig. 3. RMSD, RMSF, and Rg of co-crystal inhibitor (X77)-Mpro, PDT-Mpro and rutin-Mprocomplexes.

carried out by different researchers to active molecules against Mpro and PLpro (Choudhary et al., 2020; Ghosh et al., 2020; Jamalan et al., 2020; Mirza et al., 2020; Nogara et al., 2021). Medicinal plants are proposed as a favorable antiviral therapy for COVID-19 as they are reported to contain bioactive molecules that can be effective against COVID-19 (Adhikari et al., 2021; Benarba & Pandiella, 2020). Previous literature have highlighted the potential impact of medicinal plants and their phytocompounds against SARS-CoV-2 (Zannella et al., 2021; Rudrapal et al., 2021a; Rudrapal et al., 2021b). Therefore, the present study investigates a total of 225 phytocompounds present in 28 different Indian spices for their inhibitory potential against Mpro and PLpro of SARS-CoV-2 through computational investigations.

The catalytic sites of Mpro and Plpro are essential for active residues of protein molecule and and chemical groups of ligands (Ismail et al., 2021; Osipiuk et al., 2021; Kneller, Phillips, O'Neill, et al., 2020; Kneller et al., 2020). Studies reported that thioflavonoids, epicatechin-3-O-gallate, dobutamine and masoprocol interacted with (binding sites) Mpro and PLpro, and were considered as SARS-CoV-2 inhibitors (Kneller, Phillips, Weiss, et al., 2020; Liu et al., 2020; Ismail et al., 2021). Thus, bioactive molecules bind to or interact with the active residues which are present at the binding cavity of Mpro and PLpro.

From the present computational investigations, we found that PDT showed the best binding affinity (XP glide score: −15.367) for the binding cavity of Mpro. PDT interacted with the binding site of Mpro as it produced a conventional H-bond with CYS145 and hydrophobic interaction with HIS41. Among the residues present at the active site cavity, PDT also bonded through H-bonds with GLU166, and GLN189, while Van der Waals interactions were shown by SER46, ASN142, PRO168, and THR190. From MD simulation, it was observed that PDT showed stable conformation at the catalytic site throughout the entire simulation as evidenced by small fluctuations in the RMSD, RMSF, and Rg values. However, it showed the highest binding free energy (-280.170 ± 18.945) among the tested compounds against Mpro. Based on ADMET studies, PDT was predicted to have low oral bioavailability. However, PDT was computed to be safe for oral consumption as its LD_{50} was predicted to be 2260 mg/kg. The synthetic accessibility score of PDT was computed to be 8.43 which suggest that the compound might be difficult to synthesize. A score of 1 indicates easier synthesis, while a score of 10 indicates difficulty in synthesis (Daina et al., 2017).

With an XP glide score of −12.360, the present computational investigation found rutin as a phytocompound of Indian spices that showed the second most binding affinity for the active site of Mpro. Rutin formed bonds with the residues from the binding cavity of Mpro as it produced H-bonds with CSY145 and a C-H bond with HIS41. Among the other amino acids present at the catalytic site cavity, rutin was reported to form a conventional H-bond with GLU166; C-H bond with LEU141 and ASN142; and Van der Waals

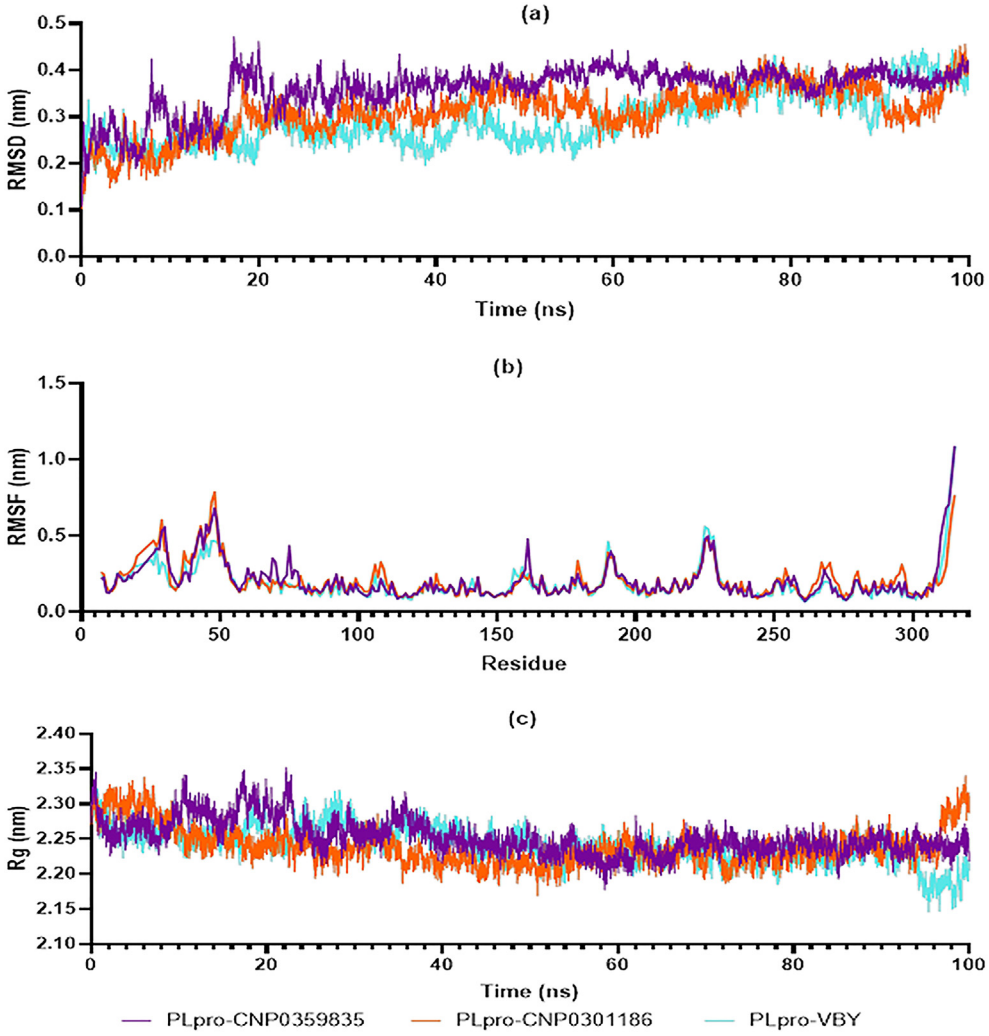

Fig. 4. RMSD, RMSF, and Rg of co-crystal inhibitor (VBY)-PLpro, luteolin-7-glucoside-4′-neohesperidoside-PLpro and DOC-PLpro complexes.

Table 2
MM-PBSA binding energies of complexes.

Parameters	Mpro-X77 (kJ/mol)	Mpro-PDT (kJ/mol)	Mpro-rutin (kJ/mol)
Van der Waals	−233.832 ± 13.802	−355.510 ± 17.262	−211.393 ± 14.098
Electrostatic	−29.776 ± 6.919	−29.163 ± 6.227	−13.087 ± 5.129
Polar solvation	123.945 ± 13.577	135.832 ± 13.738	98.523 ± 9.361
SASA	−20.961 ± 1.249	−31.329 ± 1.393	−20.863 ± 1.470
Binding free energy	−160.625 ± 15.840	−280.170 ± 18.945	−146.820 ± 15.448

Mpro: main protease; PLpro: papain-like protease.
MM-PBSA: Molecular mechanics Poisson–Boltzmann surface area.
SASA: solvent-accessible surface area.

Table 3
MM-PBSA binding energies of complexes.

Parameters	PLpro-VBY (kJ/mol)	PLpro-DOC (kJ/mol)	PLpro- luteolin-7-glucoside-4′-neohesperidoside (kJ/mol)
Van der Waals	−184.421 ± 12.283	−191.426 ± 16.939	−214.400 ± 12.998
Electrostatic	−33.836 ± 8.954	−6.045 ± 3.906	−8.373 ± 7.114
Polar solvation	94.347 ± 8.732	69.799 ± 13.131	101.490 ± 24.329
SASA	−17.663 ± 0.935	20.651 ± 1.724	−21.141 ± 1.784
Binding free energy	−141.573 ± 13.971	−148.323 ± 15.338	−142.425 ± 22.452

Mpro: main protease; PLpro: papain-like protease.
MM-PBSA: Molecular mechanics Poisson–Boltzmann surface area.
SASA: solvent-accessible surface area.

Table 4
ADMET parameters of compounds.

Properties	PDT	Rutin	DOC	Luteolin-7-Glucoside-4′-Neohesperidoside
Lipinski's rule violations	3	3	3	3
Bioavailability score	0.17	0.17	0.17	0.17
Synthetic accessibility	8.43	6.52	6.54	7.48
LD_{50} (mg/kg)	2260	5000	5000	5000
Toxicity class	5	5	5	5
Drug score	0.2016708	0.546604	0.1766791	0.1573803

ADMET: absorption, distribution, metabolism, excretion, and toxicity.
LD: Lethal Dose.

interactions were shown by SER46, GLN189, and THR190. The RMSD, RMSF, and Rg data generated from the 100 ns MD simulation indicate that the docked ligand (rutin) is stable throughout the entire simulation because the observed fluctuations were minimal (Prajapati et al., 2021). The binding free energy released during Mpro-rutin interaction was computed to be −146.820 ± 15.448 kJ/mol. Rutin showed a lower binding free energy as compared to PDT (-280.170 ± 18.945 kJ/mol) which implies that the MM-PBSA calculation for rutin supports the results of the MD simulation that had previously suggested a stable Mpro-rutin binding. Moreover, the binding free energy of rutin was also found to be lower than the co-crystal ligand 'X77' (-160.625 ± 15.840 kJ/mol). Rutin was computed by SwissADME (Daina et al., 2017) as a phytocompound with low bioavailability (Bioavailability score = 0.17). However, rutin (6.53) was predicted to be easier to be synthesized as compared to PDT (8.43). ProTox-II (Banerjee et al., 2018) predicted rutin as safe for oral consumption with an LD_{50} of 5000 mg/kg body weight. DataWarrior software-generated overall drug score for rutin was 0.546604 and was the highest among all the studied phytocompounds, even higher than that of PDT (0.2016708).

The XP glide score of DOC against PLpro was −12.801. DOC had the best binding affinity towards PLpro among all the compounds present in Indian spices. Among the amino acids at the active binding site, TYR268 and GLN269 showed Van der Waals's interaction with DOC. DOC also formed conventional H-bonds with ASP164, GLU167, PRO248, GLY266, and ASN267. Minimum fluctuations are desirable with the parameters generated from MD simulation. The RMSD, RMSF, and Rg trajectories of the PLpro-DOC complex showed small fluctuations. This is indicative of a stable protein–ligand interaction. Considering the binding free energy, the PLpro-DOC (148.323 ± 15.338 kJ/mol) outperforms the protein-native ligand complex (141.573 ± 13.971 kJ/mol). The low binding free energy of the PLpro-DOC complex supports the findings from the MD simulation. DOC violated 3 parameters (mw more than 500, H-bond acceptor more than 10, H-bond donor more than 5) in rule of 5 defined by Lipinski (Lipinski, 2004) and showed a low bioavailability score of 0.17. DOC has a synthetic accessibility score of 6.54. The LD_{50} and toxicity class of DOC were 5000 mg/kg and 5, respectively. This suggests that although DOC will be safe for oral consumption, it will have low bioavailability. The overall drug score of DOC as computed by Data Warrior software was 0.1766791. The drug score of DOC was lower than rutin (0.546604) and PDT (0.2016708).

Luteolin-7-glucoside-4′-neohesperidoside had a binding affinity score of −9.226 with PLpro. It was the phytocompound that showed the second most binding affinity towards PLpro next to DOC. Among the amino acids present at the active binding site, luteolin-7-glucoside-4′-neohesperidoside interacted with TYR268 (hydrophobic interaction) and GLN269 (C-H bond). The compound also formed conventional H-bonds with LYS157, GLU161, ASP164, GLU167, ARG166, and THR301. During MD simulation, the interaction was found to be stable as fewer fluctuations were observed in the RMSD, RMSF, and Rg trajectories. Moreover, the binding free energy of luteolin-7-glucoside-4′-neohesperidoside (-142.425 ± 22.452 kJ/mol) was lower than the native ligand (-141.573 ± 13.971 kJ/mol). The MM-PBSA calculations support the results of the MD simulation. Similar to DOC, luteolin-7-glucoside-4′-neohesperido side also showed the same violations against Lipinski's rule of 5 (Lipinski, 2004), had a low bioavailability score of 0.17. The LD_{50} was reported 5000 mg/kg with a toxicity level of 5. This reveals that luteolin-7-glucoside-4′-neohesperidoside will have low bioavailability but will be safe for oral consumption (Rudrapal et al., 2021a, 2021b). The synthetic accessibility score of the compound was 7.48. Luteolin-7-glucoside-4′-neohesperidoside will be more difficult to be synthesized than DOC (6.54). Also, luteolin-7-glucoside-4′-neohesperidoside has the lowest drug score (0.1573803) among all the studied phytocompounds.

The bioavailability issues that might arise with PDT, rutin, DOC, and luteolin-7-glucoside-4′-neohesperidoside can be effectively solved with novel drug delivery systems such as nanoformulations since it was reported that bioavailability enhancement was achieved for antiviral drugs through nanoformulation strategy (Tatham et al., 2015). The present study identifies rutin and luteolin-7-glucoside-4′-neohesperidoside as potential inhibitors of Mpro and PLpro, respectively. Other studies have also reported rutin as SARS-CoV-2 Mpro inhibitor (Huynh et al., 2020; Zothantluanga, 2021; Zothantluanga et al., 2022). The findings of our current study support similar studies conducted earlier by other researchers.

5. Conclusions

From computational investigations, among 225 phytocompounds that are present in 28 different Indian spices, four bioactive compounds viz., PDT, rutin, DOC, and luteolin-7-glucoside-4′-neo hesperidoside were identified. These four compounds exhibited promising inhibitory potential against SARS-CoV-2 Mpro and PLpro. Further experimental studies with the identified phytocompounds from Indian spices can be carried out in order to further explore their anti-SARS-CoV-2 potential.

Funding

There are no financial and personal relationships with other people or organizations that could inappropriately influence (bias) the outcomes of the present study.

CRediT authorship contribution statement

Mithun Rudrapal: Conceptualization, Methodology, Writing – original draft, Writing – review & editing. **Ismail Celik:** Methodology, Software, Data curation, Validation. **Sampath Chinnam:** Visualization, Investigation. **Mohammad Azam Ansari:** Funding acquisition, Writing – review & editing. **Johra Khan:** Funding acquisition, Writing – review & editing. **Saad Alghamdi:** Funding acquisition, Writing – review & editing. **Mazen Almehmadi:** Fund-

ing acquisition, Writing – review & editing. **James H. Zothantluanga:** Methodology. **Shubham J. Khairnar:** Visualization, Investigation.

Declaration of Competing Interest

The authors declare that they have no known competing financial interests or personal relationships that could have appeared to influence the work reported in this paper.

Acknowledgments

The authors express their sincere thanks to Taif University, Taif, Saudi Arabia for their support through Taif University Researchers Supporting Project Number: TURSP-2020/80. The authors would like to thank Ankara University-Scientific Research Unit for providing computational facility (Schrödinger software) under the grant project number BAP-21B0237004.

References

Abraham, M.J., Murtola, T., Schulz, R., Páll, S., Smith, J.C., Hess, B., Lindahl, E., 2015. GROMACS: High performance molecular simulation through multi-level parallelism from laptops to supercomputers. SoftwareX 1, 19–25. https://doi.org/10.1016/j.softx.2015.06.001.

Adhikari, B., Marasini, B.P., Rayamajhee, B., Bhattarai, B.R., Lamichhane, G., Khadayat, K., Adhikari, A., Khanal, S., Parajuli, N., 2021. Potential roles of medicinal plants for the treatment of viral diseases focusing on COVID-19: A review. Phytother. Res. 35 (3), 1298–1312. https://doi.org/10.1002/ptr.6893.

Banerjee, P., Eckert, A.O., Schrey, A.K., Preissner, R., 2018. ProTox-II: a webserver for the prediction of toxicity of chemicals. Nucleic Acids Res. 46 (W1), W257–W263. https://doi.org/10.1093/nar/gky318.

Benarba, B., Pandiella, A., 2020. Medicinal plants as sources of active molecules against COVID-19. Front. Pharmacol. 11, 1189. https://doi.org/10.3389/fphar.2020.01189.

Bhat, E.A., khan, J., Sajjad, N., Ali, A., Aldakeel, F.M., Mateen, A., Alqahtani, M.S., Syed, R., 2020. SARS-CoV-2: insight in genome structure, pathogenesis and viral receptor binding analysis–an updated review. Int. Immunopharmacol. 95, 107493. https://doi.org/10.1016/j.intimp.2021.107493.

Chen, I.J., Foloppe, N., 2010. Drug-like bioactive structures and conformational coverage with the LigPrep/ConfGen suite: comparison to programs MOE and catalyst. J. Chem. Inf. Model. 50 (5), 822–839. https://doi.org/10.1021/ci100026x.

Choudhary, M.I., Shaikh, M., tul-Wahab, A., ur-Rahman, A., Salahub, D., 2020. In silico identification of potential inhibitors of key SARS-CoV-2 3CL hydrolase (Mpro) via molecular docking, MMGBSA predictive binding energy calculations, and molecular dynamics simulation. PLoS One. 15 (7), e0235030. https://doi.org/10.1371/journal.pone.0235030.

Daina, A., Michielin, O., Zoete, V., 2017. SwissADME: a free web tool to evaluate pharmacokinetics, drug-likeness and medicinal chemistry friendliness of small molecules. Sci. Rep. 7 (1), 1–13. https://doi.org/10.1038/srep42717.

Dong, E., Du, H., Gardner, L., 2020. An interactive web-based dashboard to track COVID-19 in real time. Lancet Infect. Dis. 20 (5), 533–534. https://doi.org/10.1016/s1473-3099(20)30120-1.

Dror, A.A., Eisenbach, N., Taiber, S., Morozov, N.G., Mizrachi, M., Zigron, A., Srouji, S., Sela, E., 2020. Vaccine hesitancy: the next challenge in the fight against COVID-19. Eur. J. Epidemiol. 35 (8), 775–779. https://doi.org/10.1007/s10654-020-00671-y.

Embuscado, M.E., 2019. Bioactives from culinary spices and herbs: a review. J. Food Bioact. 6, 68–99. https://doi.org/10.31665/JFB.2019.6186.

Friesner, R.A., Murphy, R.B., Repasky, M.P., Frye, L.L., Greenwood, J.R., Halgren, T.A., Sanschagrin, P.C., Mainz, D.T., 2006. Extra precision glide: Docking and scoring incorporating a model of hydrophobic enclosure for protein− ligand complexes. J. Med. Chem. 49 (21), 6177–6196. https://doi.org/10.1021/jm051256o.

Ghosh, S., Chetia, D., Gogoi, N., Rudrapal, M., 2021. Design, Molecular Docking, Drug-likeness and Molecular Dynamics Studies of 1,2,4-Trioxane Derivatives as Novel P. falciparum Falcipain-2 (FP-2) Inhibitors. Biotechnologia 102 (3), 257–275. https://doi.org/10.5114/bta.2021.108722.

Ghosh, R., Chakraborty, A., Biswas, A., Chowdhuri, S., 2020. Evaluation of green tea polyphenols as novel corona virus (SARS CoV-2) main protease (Mpro) inhibitors–an in silico docking and molecular dynamics simulation study. J. Biomol. Struct. Dyn. 39 (12), 4362–4374. https://doi.org/10.1080/07391102.2020.1779818.

Gowrishankar, S., Muthumanickam, S., Kamaladevi, A., Karthika, C., Jothi, R., Boomi, P., Maniazhagu, D., Pandian, S.K., 2021. Promising phytochemicals of traditional Indian herbal steam inhalation therapy to combat COVID-19–An in silico study. Food Chem. Toxicol. 148, 111966. https://doi.org/10.1016/j.fct.2020.111966.

Halgren, T.A., Murphy, R.B., Friesner, R.A., Beard, H.S., Frye, L.L., Pollard, W.T., Banks, J.L., 2004. Glide: a new approach for rapid, accurate docking and scoring. 2. Enrichment factors in database screening. J. Med. Chem. 47 (7), 1750–1759. https://doi.org/10.1021/jm030644s.

Hassan Baig, M., Ahmad, K., Roy, S., Mohammad Ashraf, J., Adil, M., Haris Siddiqui, M., Khan, S., Amjad Kamal, M., Provazník, I., Choi, I., 2016. Computer aided drug design: success and limitations. Curr. Pharm. Des. 22 (5), 572–581. https://doi.org/10.2174/1381612822666151125000550.

Hevener, K.E., Zhao, W., Ball, D.M., Babaoglu, K., Qi, J., White, S.W., Lee, R.E., 2009. Validation of molecular docking programs for virtual screening against dihydropteroate synthase. J. Chem. Inf. Model. 49 (2), 444–460. https://doi.org/10.1021/ci800293n.

Humphrey, W., Dalke, A., Schulten, K., 1996. VMD: visual molecular dynamics. J. Mol. Graph. 14 (1), 33–38. https://doi.org/10.1016/0263-7855(96)00018-5.

Huynh, T., Wang, H., Luan, B., 2020. Structure-based lead optimization of herbal medicine rutin for inhibiting SARS-CoV-2's main protease. Phys. Chem. Chem. Phys. 22 (43), 25335–25343. https://doi.org/10.1039/d0cp03867a.

Ismail, M.I., Ragab, H.M., Bekhit, A.A., Ibrahim, T.M., 2021. Targeting multiple conformations of SARS-CoV2 Papain-Like Protease for drug repositioning: An in-silico study. Comput. Biol. Med. 131, 104295. https://doi.org/10.1016/j.compbiomed.2021.104295.

Jamalan, M., Barzegari, E., Gholami-Borujeni, F., 2020. Structure-Based Screening to Discover New Inhibitors for Papain-like Proteinase of SARS-CoV-2: An *In Silico* Study. J. Proteome Res. 20 (1), 1015–1026. https://doi.org/10.1021/acs.jproteome.0c00836.

James, A.E., Okoro, U.C., Ezeokonkwo, M.A., Bhimapaka, C.R., Rudrapal, M., Ugwu, D. I., Gogoi, N., Chetia, D., Celik, I., 2022. Design, synthesis, molecular docking, molecular dynamics and *in vivo* antimalarial activity of new dipeptide-sulfonamides. Chem. Select. 7 (5). https://doi.org/10.1002/slct.202103908.

Junejo, J.A., Zaman, K., Rudrapal, M., Celik, I., Attah, E.I., 2021. Antidiabetic bioactive compounds from *Tetrastigma angustifolia* (Roxb.) Deb and Oxalis debilis Kunth.: Validation of ethnomedicinal claim by *in vitro* and *in silico* studies. South African J. Bot. 143, 164–173. https://doi.org/10.1016/j.sajb.2021.07.023.

Kalita, J., Chetia, D., Rudrapal, M., 2020. Design, Synthesis, Antimalarial Activity and Docking Study of 7-Chloro-4-(2-(substituted benzylidene)hydrazineyl) quinolines. Med. Chem. 16 (7), 928–937. https://doi.org/10.2174/1573406415666190806154722.

Khan, J., Asoom, L.I.A., Khan, M., Chakrabartty, I., Dandoti, S., Rudrapal, M., Zothantluanga, J.H., 2021. Evolution of RNA viruses from SARS to SARS-CoV-2 and diagnostic techniques for COVID-19: a review. Beni Suef Univ. J. Basic Appl. Sci. 10 (1), 1–14. https://doi.org/10.1186/s43088-021-00150-7.

Kneller, D.W., Phillips, G., O'Neill, H.M., Jedrzejczak, R., Stols, L., Langan, P., Joachimiak, A., Coates, L., Kovalevsky, A., 2020a. Structural plasticity of SARS-CoV-2 3CL M pro active site cavity revealed by room temperature X-ray crystallography. Nat. Commun. 11 (1), 3202. https://doi.org/10.1038/s41467-020-16954-7.

Kneller, D.W., Phillips, G., Weiss, K.L., Pant, S., Zhang, Q., O'Neill, H.M., Coates, L., Kovalevsky, A., 2020b. Unusual zwitterionic catalytic site of SARS–CoV-2 main protease revealed by neutron crystallography. J. Biol. Chem. 295 (50), 17365–17373. https://doi.org/10.1074/jbc.ac120.016154.

Kumar, D., Jahan, S., Khan, A., Siddiqui, A.J., Redhu, N.S., Wahajuddin, Khan, J., Banwas, S., Alshehri, B., Alaidarous, M., 2021a. Neurological Manifestation of SARS-CoV-2 Induced Inflammation and Possible Therapeutic Strategies Against COVID-19. Mol. Neurobiol. 58 (7), 3417–3434. https://doi.org/10.1007/s12035-021-02318-9.

Kumar, P.P., Shaik, R.A., Khan, J., Alaidarous, M.A., Rudrapal, M., Khairnar, S.J., Sahoo, R., Zothantluanga, J.H., Walode, S.G., 2021b. Cerebroprotective Effect of Aloe Emodin. Saudi J. Biol. Sci. 29 (2), 998–1005. https://doi.org/10.1016/j.sjbs.2021.09.077.

Kumar, Y., Singh, H., Patel, C.N., 2020. *In silico* prediction of potential inhibitors for the main protease of SARS-CoV-2 using molecular docking and dynamics simulation based drug-repurposing. J. Infect. Public Health. 13 (9), 1210–1223. https://doi.org/10.1016/j.jiph.2020.06.016.

Kumari, R., Kumar, R., Lynn, A., 2014. g_mmpbsa- A GROMACS tool for high-throughput MM-PBSA calculations. J. Chem. Inf. Model. 54 (7), 1951–1962. https://doi.org/10.1021/ci500020m.

Lipinski, C.A., 2004. Lead-and drug-like compounds: the rule-of-five revolution. Drug Discov. Today. Technol. 1 (4), 337–341. https://doi.org/10.1016/j.ddtec.2004.11.007.

Liu, Y.C., Kuo, R.L., Shih, S.R., 2020. COVID-19: The first documented coronavirus pandemic in history. Biomed. J. 43 (4), 328–333. https://doi.org/10.1016/j.bj.2020.04.007.

Lucia, V.C., Kelekar, A., Afonso, N.M., 2021. COVID-19 vaccine hesitancy among medical students. J. Public Health. 43 (3), 445–449. https://doi.org/10.1093/pubmed/fdaa230.

Mirza, M.U., Ahmad, S., Abdullah, I., Froeyen, M., 2020. Identification of novel human USP2 inhibitor and its putative role in treatment of COVID-19 by inhibiting SARS-CoV-2 papain-like (PLpro) protease. Comput. Biol. Chem. 89, 107376. https://doi.org/10.1016/j.compbiolchem.2020.107376.

Mohamadian, M., Chiti, H., Shoghli, A., Biglari, S., Parsamanesh, N., Esmaeilzadeh, A., 2021. COVID-19: Virology, biology and novel laboratory diagnosis. J. Gene Med. 23, (2). https://doi.org/10.1002/jgm.3303 e3303.

Nogara, P.A., Omage, F.B., Bolzan, G.R., Delgado, C.P., Aschner, M., Orian, L., Teixeira Rocha, J.B., 2021. In silico Studies on the Interaction Between Mpro and PLpro From SARS-CoV-2 and Ebselen, its Metabolites and Derivatives. Mol. Inform. 40, (8). https://doi.org/10.1002/minf.202100028 e2100028.

Opara, E.I., Chohan, M., 2014. Culinary herbs and spices: their bioactive properties, the contribution of polyphenols and the challenges in deducing their true health benefits. Int. J. Mol. Sci. 15 (10), 19183–19202. https://doi.org/10.3390/ijms151019183.

Osipiuk, J., Azizi, S.-A., Dvorkin, S., Endres, M., Jedrzejczak, R., Jones, K.A., Kang, S., Kathayat, R.S., Kim, Y., Lisnyak, V.G., Maki, S.L., Nicolaescu, V., Taylor, C.A., Tesar, C., Zhang, Y.-A., Zhou, Z., Randall, G., Michalska, K., Snyder, S.A., Dickinson, B.C., Joachimiak, A., 2021. Structure of papain-like protease from SARS-CoV-2 and its complexes with non-covalent inhibitors. Nat. Commun. 12 (1). https://doi.org/10.1038/s41467-021-21060-3.

Othman, I.M., Mahross, M.H., Gad-Elkareem, M.A., Rudrapal, M., Gogoi, N., Chetia, D., Aouadi, K., Snoussi, M., Kadri, A., 2021. Toward a treatment of antibacterial and antifungal infections: Design, synthesis and in vitro activity of novel arylhydrazothiazolylsulfonamides analogues and their insight of DFT, docking and molecular dynamic simulation. J. Mol. Struct. 1243. https://doi.org/10.1016/j.molstruc.2021.130862.

Pasala, P.K., Siva Reddy, S.S.L., Silvia, N., Reddy, D.Y., Sampath, A., Dorababu, N., Sirisha Mulukuri, N.V.L., Sunil Kumar, K.T., Chandana, S.M., Chetty, M.C., Bendale, A.R., Rudrapal, M., 2022. *In vivo* immunomodulatory activity and *In silico* study of *Albizia procera* bark extract on doxorubicin induced immunosuppressive rats. J. King Saud Univ. Sci. 34, (3). https://doi.org/10.1016/j.jksus.2022.101828 101828.

Prajapati, J., Patel, R., Goswami, D., Saraf, M., Rawal, R.M., 2021. Sterenin M as a potential inhibitor of SARS-CoV-2 main protease identified from MeFSAT database using molecular docking, molecular dynamics simulation and binding free energy calculation. Comput. Biol. Med. 135, 104568. https://doi.org/10.1016/j.compbiomed.2021.104568.

Rath, B., Abul Qais, F., Patro, R., Mohapatra, S., Sharma, T., 2021. Design, synthesis and molecular modeling studies of novel mesalamine linked coumarin for treatment of inflammatory bowel disease. Bioorg. Med. Chem. Lett. 41, 128029. https://doi.org/10.1016/j.bmcl.2021.128029.

Riad, A., 2021. Oral side effects of COVID-19 vaccine. Br. Dent. J. 230 (2), 59. https://doi.org/10.1038/s41415-021-2615-x.

Roos, K., Wu, C., Damm, W., Reboul, M., Stevenson, J.M., Lu, C., Dahlgren, M.K., Mondal, S., Chen, W., Wang, L., Abel, R., Friesner, R.A., Harder, E.D., 2019. OPLS3e: Extending force field coverage for drug-like small molecules. J. Chem. Theory Comput. 15 (3), 1863–1874. https://doi.org/10.1021/acs.jctc.8b01026.

Rudrapal, M., Issahaku, A.R., Agoni, C., Bendale, A.R., Nagar, A., Soliman, M.E., Lokwani, D., 2021a. *In silico* screening of phytopolyphenolics for the identification of bioactive compounds as novel protease inhibitors effective against SARS-CoV-2. J. Biomol. Struct. Dyn. 1–17. https://doi.org/10.1080/07391102.2021.1944909.

Rudrapal, M., Khairnar, S.J., Borse, L.B., Jadhav, A.J., 2020. Coronavirus disease-2019 (COVID-19): An updated review. Drug Res. 70 (9), 389–400. https://doi.org/10.1055/a-1217-2397.

Rudrapal, M., Gogoi, N., Chetia, D., Khan, J., Banwas, S., Alshehri, B., Alaidarous, M.A., Laddha, U.D., Khairnar, S.J., Walode, S.G., 2021b. Repurposing of Phytomedicine-Derived Bioactive Compounds With Promising Anti-SARS-CoV-2 Potential: Molecular Docking, MD Simulation and Drug-Likeness/ADMET Studies. Saudi J. Biol. Sci. https://doi.org/10.1016/j.sjbs.2021.12.018.

Rudrapal, M., Celik, I., Khan, J., Ansari, M.A., Alomary, M.N., Alatawi, F.A., Yadav, R., Sharma, T., Tallei, T.E., Pasala, P.K., Sahoo, R.K., Khairnar, S.J., Bendale, A.R., Zothantluanga, J.H., Chetia, D., Walode, S.G., 2022. Identification of bioactive molecules from *Triphala* (Ayurvedic herbal formulation) as potential inhibitors of SARS-CoV-2 main protease (Mpro) through computational investigations. J. King Saud Univ. Sci. 34 (3), 101826. https://doi.org/10.1016/j.jksus.2022.101826.

Sachdeva, C., Wadhwa, A., Kumari, A., Hussain, F., Jha, P., Kaushik, N.K., 2020. In silico potential of approved antimalarial drugs for repurposing against COVID-19. OMICS 24 (10), 568–580. https://doi.org/10.1089/omi.2020.0071.

Shah, B., Modi, P., Sagar, S.R., 2020. In silico studies on therapeutic agents for COVID-19: Drug repurposing approach. Life Sci. 252, 117652. https://doi.org/10.1016/j.lfs.2020.117652.

Srinivasan, K., 2005. Role of spices beyond food flavoring: Nutraceuticals with multiple health effects. Food Rev. Int. 21 (2), 167–188. https://doi.org/10.1081/FRI-200051872.

Swargiary, A., Mahmud, S., Saleh, M.A., 2020. Screening of phytochemicals as potent inhibitor of 3-chymotrypsin and papain-like proteases of SARS-CoV2: an in silico approach to combat COVID-19. J. Biomol. Struct. Dyn. 1–15. https://doi.org/10.1080/07391102.2020.1835729.

Tatham, L.M., Rannard, S.P., Owen, A., 2015. Nanoformulation strategies for the enhanced oral bioavailability of antiretroviral therapeutics. Ther. Deliv. 6 (4), 469–490. https://doi.org/10.4155/tde.15.4.

Yashin, A., Yashin, Y., Xia, X., Nemzer, B., 2017. Antioxidant activity of spices and their impact on human health: A review. Antioxidants 6 (3), 70. https://doi.org/10.3390/antiox6030070.

Zannella, C., Giugliano, R., Chianese, A., Buonocore, C., Vitale, G.A., Sanna, G., Sarno, F., Manzin, A., Nebbioso, A., Termolino, P., Altucci, L., Galdiero, M., de Pascale, D., Franci, G., 2021. Antiviral Activity of Vitis vinifera Leaf Extract against SARS-CoV-2 and HSV-1. Viruses 13 (7), 1263. https://doi.org/10.3390/v13071263.

Zothantluanga, J.H., 2021. Molecular Docking Simulation Studies, Toxicity Study, Bioactivity Prediction, and Structure-Activity Relationship Reveals Rutin as a Potential Inhibitor of SARS-CoV-2 3CL pro. J. Sci. Res. 65 (5), 96–104. https://doi.org/10.37398/JSR.2021.650511.

Zothantluanga, J.H., Aswin, S.K., Rudrapal, M., Cheita, D., 2022. Antimalarial flavonoid-glycoside from Acacia pennata against PfDHFR-TS: An *in-silico* study. Biointerface Res. Appl. Chem. 12 (4), 4871–4887. https://doi.org/10.33263/BRIAC124.48714887.